Science of the Total Environment 861 (2023) 160624

Contents lists available at ScienceDirect

Science of the Total Environment

journal homepage: www.elsevier.com/locate/scitotenv

Humic acid controls cadmium stabilization during Fe(II)-induced lepidocrocite transformation

Hongling Bu [a,b,1], Qinkai Lei [a,b,1], Hui Tong [a], Chengshuai Liu [c], Shujie Hu [a], Wenpo Xu [a], Yujie Wang [b], Manjia Chen [a,*], Jiangtao Qiao [a]

[a] National-Regional Joint Engineering Research Center for Soil Pollution Control and Remediation in South China, Guangdong Key Laboratory of Integrated Agro-environmental Pollution Control and Management, Institute of Eco-environmental and Soil Sciences, Guangdong Academy of Sciences, Guangzhou 510650, China
[b] School of Environmental Science and Engineering, Guangdong University of Technology, Guangzhou 510006, China
[c] State Key Laboratory of Environmental Geochemistry, Institute of Geochemistry, Chinese Academy of Sciences, Guiyang 550081, China

HIGHLIGHTS

- Magnetite was formed during Fe(II)-induced transformation of lepidocrocite (Lep).
- Humic acid inhibited Lep transformation with increasing C/Fe ratios.
- Fe(II)-induced transformation of Lep was beneficial for binding Cd(II).
- Cd(II) could be immobilized in the newly formed magnetite structure.
- Humic acid affected Cd(II) transformation during Fe(II)-induced transformation of Lep-HA.

GRAPHICAL ABSTRACT

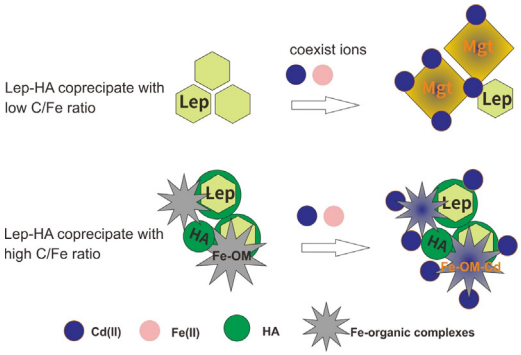

ARTICLE INFO

Editor: Baoliang Chen

Keywords:
Lepidocrocite
Humic acid
Mineral transformation
Cd(II)
Immobilization

ABSTRACT

Abiotic reduction of iron (oxyhydr)oxides by aqueous Fe(II) is one of the key processes affecting the Fe cycle in soil. Lepidocrocite (Lep) occurs naturally in anaerobic, clayey, non-calcareous soils in cooler and temperate regions; however, little is known about the impacts of co-precipitated humic acid (HA) on Fe(II)-induced Lep transformation and its consequences for heavy metal immobilization. In this study, the Fe(II)-induced phase transformation of Lep-HA co-precipitates was analyzed as a function of the C/Fe ratio, and its implications for subsequent Cd(II) concentration dynamic in dissolved and solid form was further investigated. The results revealed that secondary Fe(II)-bearing magnetite commonly formed during the Fe(II)-induced transformation of Lep, which further changed the mobility and distribution of Cd(II). The co-precipitated HA resulted in a decrease in the Fe solid phase transformation as the C/Fe ratios increased. Magnetite was found to be a secondary mineral in the 0.3C/Fe ratio Lep-HA co-precipitate, while only Lep was observed at a C/Fe ratio of 1.2 using X-ray diffraction (XRD) and Mössbauer spectroscopy. Based on XRD, scanning electron microscopy (SEM), Mössbauer, X-ray photoelectron spectroscopy (XPS), and Fourier transform infrared spectroscopy (FTIR) results, newly formed magnetite may immobilize Cd(II) through surface complexes, incorporation, or structural substitution. The presence of HA was beneficial for binding Cd(II) and affected the mineralogical transformation of Lep into magnetite, which further induced the distribution of Cd(II) into the newly formed secondary minerals. These results provide insights into the behavior of Cd(II) in response to reaction between humic matter and iron (oxyhydr)oxides in anaerobic environments.

* Corresponding author at: No. 808 Tianyuan Road, Tianhe District, Guangzhou 510650, China.
E-mail address: mjchen@soil.gd.cn (M. Chen).
[1] These authors contributed equally to this work.

http://dx.doi.org/10.1016/j.scitotenv.2022.160624
Received 13 September 2022; Received in revised form 14 November 2022; Accepted 27 November 2022
Available online 29 November 2022

1. Introduction

Iron (oxyhydr)oxides are common minerals in soil environments (Kappler et al., 2021). Due to their nanoscale structure, higher surface area, and available reactive sites, iron (oxyhydr)oxide plays an important role in the geochemical cycles of nutrients and heavy metals (e.g., cadmium), influencing their chemical speciation and behavior in soils and sediments (Karimian et al., 2019). Nonetheless, iron (oxyhydr)oxides rarely exist alone in natural environments and generally coexist with inorganic or organic components (Bao et al., 2021; Kappler et al., 2021). For instance, ferrihydrite often coexists with aqueous Fe(II) at the different redox interfaces in soils and sediments, which induces redox reactions and leads to the formation of secondary Fe minerals (Liu et al., 2016). Moreover, due to the various functional groups of organic matter (OM), such as carboxyl groups (–COOH) and phenolic hydroxyl groups (–OH), iron (oxyhydr)oxides tend to adsorb or complex with OM to form Fe-OM associations (Bao et al., 2021; Chen et al., 2014a; Kleber et al., 2015). Thus, these reactions among Fe(II), iron (oxyhydr)oxides, and OM could further affect the mobility or availability of heavy metals in the surrounding environments.

The effects of reactions between Fe(II) and iron (oxyhydr)oxides on the transformation of Fe minerals and the redistribution of trace metals have been well reported (Latta et al., 2012; Liu et al., 2016). In sub-anoxic or anoxic soils, iron (oxyhydr)oxides, such as ferrihydrite would transform to more crystalline Fe minerals via abiotic catalysis with Fe(II) (Kappler et al., 2021; Liu et al., 2016; Schulz et al., 2022). These mineral recrystallization and transformation processes may lead to changes in the surface and crystalline structural properties and may further affect the environmental geochemical behaviors of heavy metals and other pollutants in soils and sediments. For instance, Frierdich and Catalano (2012) investigated the Fe(II)-activated release of the trace elements Ni(II) and Zn(II) from Ni- and Zn-substituted goethite and hematite and reported that more Ni(II) was incorporated into the goethite relative to the hematite during Fe(II)-induced recrystallization. In our previous study, we also found that coexisting divalent metal cations, such as Co, Mn, Zn, and Ni, could be fixed into newly generated secondary minerals such as lepidocrocite (Lep) and goethite during the dissolution and recrystallization of ferrihydrite driven by Fe(II), thus reducing the mobility of these metals (Liu et al., 2016). Recently, Zhou et al. (2022) investigated the effects of the Fe(II)-induced transformation of scorodite on arsenic solubility and found that As(V) reduction occurred and a considerable amount of the structural As (V) was redistributed into extractable phases during the transformation of scorodite. Furthermore, Zhao et al. (2022b) investigated the fate of coexisting Cd(II) and As during the Fe(II)-induced transformation of As (V)/Cd(II)-bearing ferrihydrite and found that Cd(II) had negligible effects on the redistribution of As(V), but high concentrations of As(V) could reduce the mobility of Cd(II). Therefore, investigating the role of the reactions between Fe(II) and iron (oxyhydr)oxides on heavy metals in the environment is of great significance.

Similar to iron (oxyhydr)oxides alone, Fe-OM associations have been frequently found to be associated with the mobility and bioavailability of heavy metals in Fe(II)-based soil environments (Chen et al., 2014a; Karimian et al., 2019). The association of iron (oxyhydr)oxides with OM could change the physicochemical properties of the mineral surface (e.g., adsorption) and act as carriers to complex with metal ions (Du et al., 2018; Xu et al., 2022). Increases and decreases in the binding of heavy metals have been observed for iron (oxyhydr)oxide-humic acid composites compared to humic acid (HA) alone (Orsetti et al., 2006; Qu et al., 2022). In addition, a large number of studies have investigated the mobility and speciation of heavy metals during Fe(II)-catalyzed ferrihydrite recrystallization in the presence of OM (Karimian et al., 2019; Lu et al., 2019; Zhou et al., 2020). Karimian et al. (2019) observed copious Sb (V) reduction to Sb(III) during Fe(II)-induced ferrihydrite transformation in the presence of HA. Additionally, Zhou et al. (2020) found that co-precipitated natural OM (Suwannee River natural OM) did not significantly change the adsorption of Ni onto ferrihydrite, but the co-precipitated natural OM inhibited the transformation of the ferrihydrite and changed the fate of the Ni in the presence of Fe(II). However, these studies primarily focused on the ferrihydrite-OM complexes (Shen et al., 2022). It remains unclear whether the transformation of other iron (oxyhydr)oxides in the presence of OM affect the stability of heavy metals such as Cd.

Soil Cd pollution is a worldwide concern due to the high risks of transfer to humans through the food chain. Thus, it is necessary to gain fundamental knowledge about the migration and bioavailability of Cd in soil. Lep (γ-FeOOH), a poor crystalline iron (oxyhydr)oxide, is commonly found in anaerobic, clayey, non-calcareous soils in cooler and temperate regions (Cornell and Schwertmann, 2003), which consists of iron-centered oxygen octahedra joined by the sharing of edges into two-dimensionally infinite layers, with the successive layers held together by hydrogen bonds (Ewing, 1935). Due to the regular mineral crystal structure belonging to the rhombic system with layer structure, Lep was selected as the iron (oxyhydr)oxide probe in this study. In soil environments with relatively high levels of natural OM, Lep can become persistent through the physicochemical reaction with OM (Liu et al., 2022). Coexisting aqueous Fe(II) can induce Lep transformation to more stable iron (oxyhydr)oxides forms in anoxic environments (Schulz et al., 2022). These transformations could influence the morphologies, particle sizes, specific surface area of iron (oxyhydr)oxides, and thus control the transformation of Cd. However, up to now, few studies have focused on Fe(II)-induced transformation of Lep minerals or Lep-OM associations and its effect on the stabilization of Cd under anoxic conditions.

In this study, the reaction between aqueous Fe(II) and Lep with co-precipitated OM (C/Fe ratio of 0–1.2), and the further effect on the behavior of Cd(II) were investigated. Specifically, we investigated (i) the phase transformation of Lep and Lep-HA co-precipitates induced by Fe(II) in the presence of Cd(II), and (ii) the fate of the dissolved, extractable, and residual Cd(II) in the Lep and Lep-HA co-precipitates during the reaction. Our findings provide new insights into the fate of Cd(II) in iron (hydr)oxide -based systems that approximate natural environments.

2. Materials and methods

2.1. Synthesis of Lep and Lep-HA co-precipitates

HA (purity of 98 %) was purchased from J&K Chemicals Co. Ltd. and an HA stock solution was prepared by suspending the solid in 50 mL of Milli-Q water and adjusting the pH to ~12.0 using 0.1 mol/L KOH. The Lep was synthesized following the method described by Yen et al. (2002). For the Lep-HA co-precipitates, the Lep solutions were mixed with HA solutions first, stirred for 5 min to mix the solution evenly, and placed in a 60 °C water bath for 3 h. Then, all of the solids were washed with Milli-Q water three times and with absolute ethyl alcohol two times. Finally, the solids were heated for 48 h in a 60 °C oven. Totally, three different Fe solids were synthesized and used in this study, namely pure Lep, Lep co-precipitated with HA with a molar C/Fe ratio of 0.3 (denoted as Lep-HA-0.3), and Lep co-precipitated with HA with a C/Fe ratio of 1.2 (denoted as Lep-HA-1.2).

2.2. Cd stabilization during Fe(II)-induced Lep and Lep-HA co-precipitate transformation

All of the experiments were conducted in an anaerobic glovebox (Type A, Coy Laboratory, USA). Before the reaction, all of the solutions were aerated with N_2 (99.99 %) for >2 h, and then, they were quickly moved to the glovebox and allowed to reach equilibrium for 48 h. Six batches of experiments were conducted in this study. The reaction was carried out in a 15-mL centrifuge tube, and the polytetrafluoroethylene (PTFE) tape was wound around the screw mouth of the tube to ensure its sealing performance. Piperazine-*N*–*N*-bis-2-ethanesulfonic acid (PIPES) buffer solution, Fe(II) stock solution, Cd(II) stock solution, and Lep or Lep-HA co-precipitate were successively added to the 15-mL centrifuge tube. Then, the reaction centrifuge tube was shielded from light using tin foil and placed in the centrifuge to react (30 rpm). The reaction temperature was

25 °C. The reaction volume and pH value were 10 mL and 7.0 ± 0.1. The final concentration of each species was about 20 mmol/L Fe(III), 2 mmol/L aqueous Fe(II) ($Fe(II)_{aq}$), 25 mmol/L PIPES, and 25 mg/L Cd(II), which were selected by the representative of those found in paddy soil (Chen et al., 2014b) and previous studies (Du et al., 2018; Zhao et al., 2022a, b). The Cd(II) stock solution was prepared by dissolving appropriate amounts of $Cd(NO_3)_2$. For the control groups, Fe(II) solution or Cd(II) solution was not added, and the other conditions remained the same.

The experimental sampling times were 6 h, 1 d, 3 d, 5 d, 10 d, 15 d, and 30 d, and three parallel samples were set up for each time point. A 1.5 mL samples of the suspension was collected from each treatment and centrifuged (10,000 rpm for 15 min). The supernatant was filtered through a 0.22-μm hydrophilic syringe filter and was acidified using 5 M HCl in preparation for measuring Fe(II) and Cd(II) concentrations (dissolved $C_{Fe(II)}$ and C_{Cd}). The solid was then resuspended in 1.5 mL of sodium acetate buffer solution with a pH of 2.88 (Jing et al., 2021) and shaken for 18 h. The centrifuged supernatant was filtered and analyzed to determine the concentrations of Fe(II) and Cd(II) (extractable $C_{Fe(II)}$ and C_{Cd}). Then, the concentration of Cd(II) combined with Fe solid (residual C_{Cd}) was calculated by subtracting the concentration of aqueous Cd(II) (including extractable Cd(II) and dissolved Cd(II)) from the total concentration of Cd(II). The Cd(II) concentrations were determined via inductively coupled plasma-optical emission spectroscopy (ICP-OES, Perkin-Elmer optima 2000, USA). The Fe(II) concentrations were measured using the ferrozine method at 510 nm (Zhou et al., 2022). The solid-phase was collected from the remaining 8.5 mL of the original suspension in a tube for phase analysis via washing with Milli-Q water, centrifugation, and then freeze-drying.

2.3. Characterization of the solid phase

The X-ray diffraction (XRD) patterns for phase identification and quantification were obtained using a D8 Advanced Diffractometer (Bruker AXS). The XRD patterns were recorded over a 2θ range of 6–85° with a step size of 0.02° and a counting time of 1 s per step. The mineral phase identification was carried out by matching the obtained XRD patterns with the standard powder diffraction database (JCPDS PDF-2 database). The surface elements of the solid samples were measured using X-ray photoelectron spectrometer (XPS, Thermo Fisher Scientific K-Alpha). The excitation source was an Al Kα ray (6 eV) with a pass energy of 150 eV and a step length of 1 eV. All of the XPS patterns were acquired by setting the pass energy of the broad scans to 100 eV and narrow scans to 50 eV. The XPS results were analyzed via Gaussian fitting technology (Zhang et al., 2021; Wang et al., 2022). To evaluate the changes of phase and structure in these amorphous iron (oxyhydr)oxides during the transformation, the solid samples were also collected for ^{57}Fe-Mössbauer spectroscopy using a Wissel Elektronik (Germany) instrument with a closed-loop cryostat (CCS-850, Janis Research Co., Wilmington, MA, USA) in transmission mode with a ^{57}Co (~50 mCi) source at ~295 K (Zhou et al., 2020). The isomer shift or central point shift was calculated using 7 μm α-Fe(O) foil as the background. The data were calibrated using the α-Fe(0) foil and fitted using Mössbauer 4.0 software. The morphologies and crystallite sizes of the reacted solid samples were observed using scanning electron microscope (SEM). First, the solid samples were dispersed in absolute ethanol (≥99.5 %) and ultrasonicated, and then were deposited on holey-carbon film Cu grids. The images were then recorded using a ZEISS Gemini 300 (Germany) operated with an accelerating electrode of 0.02–30 kV and a probe beam of 3–20 nA. The surface functional groups of the solid samples were analyzed via Fourier transform infrared spectroscopy (FTIR) used using a Bruker Vertex-70 infrared spectrometer. For each measurement, the collection range of the spectrum was 400–4000 cm^{-1}, the scanning time was 32 scans, and the resolution was 4 cm^{-1}.

3. Results and discussion

3.1. Mobility and fate of Cd(II) in the different treatments

In all of the Fe(II)-bearing treatments, the dissolved Cd(II) concentrations of the three samples decreased rapidly within 1 day, and then slowly decreased to 5.5317, 4.7790 and 8.2443 mg/L after 30 days of reaction in the Lep, Lep-HA-0.3, and Lep-HA-1.2 treatments, respectively (Fig. 1b). The rapid decrease in the dissolved Cd(II) concentration in the first (about 1 day) stage was due to the formation of the inner-sphere adsorption of Cd(II) by the Lep or Lep-HA co-precipitates (Du et al., 2018; Zhou et al., 2020). The slow decrease during the following stage have been caused by the diffusion of Cd(II) into the Lep and Lep-HA co-precipitates (Scheinost et al., 2001). In addition, the Cd(II) adsorption capacity in the Lep-HA-1.2 was higher than that of the Lep-HA-0.3 and Lep due to the changes of surface charge and functional group composition of the HA (ThomasArrigo et al., 2018). A previous study also found that ferrihydrite-HA co-precipitate with high C loading exhibited a high Cd(II) sorption capacity due to surface complexation by the active functional groups in HA such as -COOH (Du et al., 2018). However, the concentrations of dissolved Cd(II) were lower in all Fe(II)-free treatments than in the Fe(II)-bearing treatments, with the following order: Lep > Lep-HA-0.3 > Lep-HA-1.2. Thus, the Fe(II) restricted the migration of the dissolved Cd(II) to the mineral surface in the binary iron (hydr)oxide-Cd and ternary iron (oxyhydr)oxides -HA-Cd systems, which will be discussed further below.

To further explore the Cd(II) distribution during the reaction, the proportions of the extractable Cd were determined at selected times (Fig. 1b and e). The concentrations of the extractable Cd(II) quickly increased within 6 h and then remained basically stable over time in both the control (Fe(II)-free) and Fe(II)-bearing treatments, with the following order: Lep-HA-1.2 > Lep-HA-0.3 > Lep. Compared to the Fe(II)-free control treatments, the concentrations of extractable Cd(II) were significantly lower in the Fe (II)-bearing treatments. The extractable Cd(II) of the Fe(II)-free treatment was 1.9 times that of the Fe(II)-bearing treatment. These results suggested that Fe(II) had an obvious effect on Cd(II) stability, and Cd(II) was more stable in the Lep and Lep-HA co-precipitates after reacted with Fe(II).

The residual Cd(II) was calculated by subtracting dissolved Cd(II) and the above described extractable Cd(II) from the total Cd(II). The concentration of the residual Cd(II) quickly increased within 1 day and remained relatively stable over time in all of the treatments (Fig. 1c and f), indicating that part of the Cd(II) was incorporated into the secondary iron minerals during the iron (oxyhydr)oxides transformation, which was similar with the previous studies (Muehe et al., 2013; Zhou et al., 2020). Muehe et al. (2013) found that Cd(II) could be immobilized by sorption to and/or coprecipitation within newly formed secondary minerals that contained Ca, Fe, and carbonate by microbially mediated turnover of Fe minerals and Fe minerals-natural OM complexes. Furthermore, the residual Cd(II) concentrations of all the Fe(II)-bearing treatments were higher than those of the Fe(II)-free treatments, with following order: Lep > Lep-HA-0.3 > Lep-HA-1.2. Similar changes in residual heavy metals remaining in the solids have been observed during Fe(II)-induced transformations of iron (oxyhydr)oxides (Shen et al., 2022). Shen et al. (2022) found residual Cd concentrations in iron (oxyhydr)oxides increased in the treatments with high Fe(II) concentrations during aging process. In this study, the equilibrated residual Cd(II) concentration of the Fe(II)-bearing treatment (17.30 mg/L) was about 1.5 times that of the Fe(II)-free treatment with Lep (10.65 mg/L). The increase in the residual Cd(II) in the Fe(II)-bearing treatments was primarily caused by the crystal phase transformation of the Lep, which was driven by the Fe(II). In the presence of HA, the residual Cd(II) concentration was substantially higher in the Fe(II)-bearing treatment samples (Lep-HA-0.3: 9.84 → 15.78 mg/L; Lep-HA-1.2: 4.95 → 10.36 mg/L) and the proportion of the residual Cd(II) decreased as the HA concentration increased, implying that the Cd(II) was incorporation into the Lep-HA co-precipitates after reaction with Fe(II) and that HA played an important role in the stability of Cd(II).

3.2. Mineralogical and morphological characteristics of the Fe-solid samples

The solid samples were characterized via XRD analysis at different sampling times for the Lep and Lep-HA co-precipitates (Fig. 2). XRD patterns showed that magnetite was initially detected after 5 days in the Fe(II) and Cd(II) treatments with Lep, and the diffraction peaks of the Lep gradually

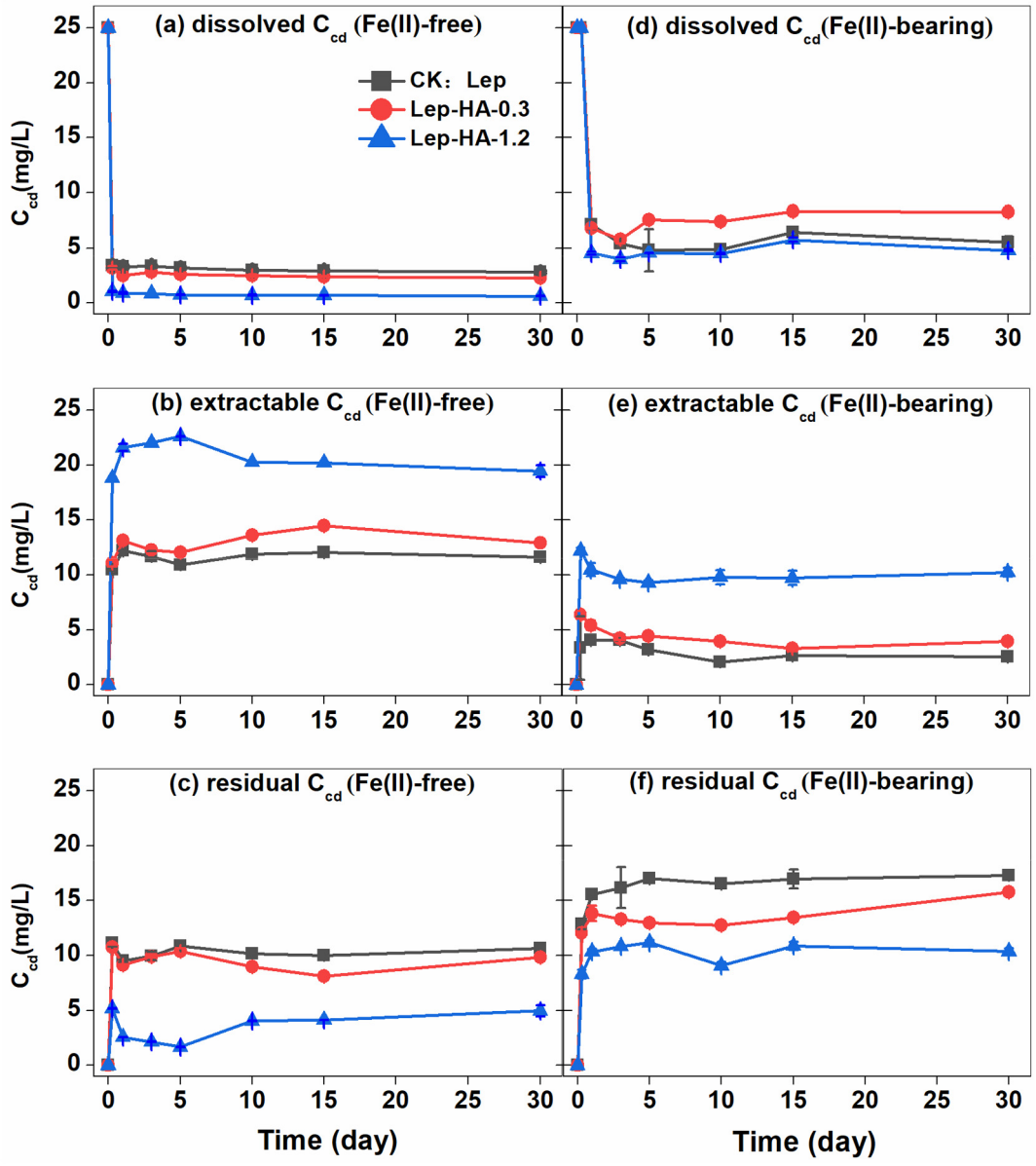

Fig. 1. Variation trend of Cd(II) concentration as a function of the reaction time. (a–c) were Fe(II)-free treatment, and (d–f) were Fe(II)-bearing treatments. (a) and (d) dissolved Cd(II), (b) and (e) extractable Cd(II), (c) and (f) residual Cd(II) concentrations for all samples without and with Fe(II) treatments, respectively. The data points represent the average value and standard deviation in triplicate bottles.

increased during the reaction (Fig. 2a). Magnetite was also detected in the treatments without addition of Cd(II) (Fig. S1). These results revealed that the crystallinity of the Lep gradually increased during the reaction, and the Fe(II) induced the transformation of Lep into the secondary Fe-phase, Lep, and magnetite (Schulz et al., 2022). However, the crystallinity of the Lep decreased in the Lep-HA co-precipitates (Fig. 2b–c), implying that some defects may have occurred in its structure. These defects in the Lep may provide a new space for metal (loid) retention (Hu et al., 2022; Lu et al., 2019). Magnetite was detected after reaction for 30 days in the Lep-HA-0.3 treatment but not in the Lep-HA-1.2 treatments with or without Cd(II) addition (Fig. 2b–c, Table. S1), suggesting that the HA inhibited the transformation of the Lep. Similar results have also been reported for the inhibition of transformation of iron (oxyhydr)oxides by some forms of OM (Sheng et al., 2020; Shen et al., 2022). HA can form stable complexes with Fe(III) in the Lep-HA co-precipitates, which creates a steric hindrance toward its polymerization into the nuclei of product the crystallites and then inhibits its subsequent Ostwald ripening and oriented aggregation due to changes in the hydrolysis and precipitation processes (Bao et al., 2021; Sheng et al., 2020; ThomasArrigo et al., 2019; Zhou et al., 2020). Although residual Cd(II) was detected in all of the samples, no significant XRD peak shift was observed in this study. This most likely resulted from the relatively small amount of structural incorporation, as well as the broadened peak (Fig. 2).

To further quantify the contents of iron (oxyhydr)oxides in the solid samples, Mössbauer spectroscopy was used to obtain the information about the electronic density at the nuclei (isomer shift, IS), the electric field gradient (quadrupole splitting, QS), and the magnetic environment (magnetic hyperfine splitting, HF). The Mössbauer spectra of the solid samples before and after reaction with and without Cd(II) are shown in Fig. 3, and the corresponding fitting parameters are presented in Table S1. The spectra before the reaction clearly showed two Fe(III) doublets with values of ~0.25 mm/s (isomer shift, IS) and ~ 0.58–0.61 mm/s (quadrupole splitting, QS) (Fig. 3a–c), indicating that the solid sample was Lep in the both Lep and Lep-HA co-precipitates (Murad and Schwertmann, 1984). The

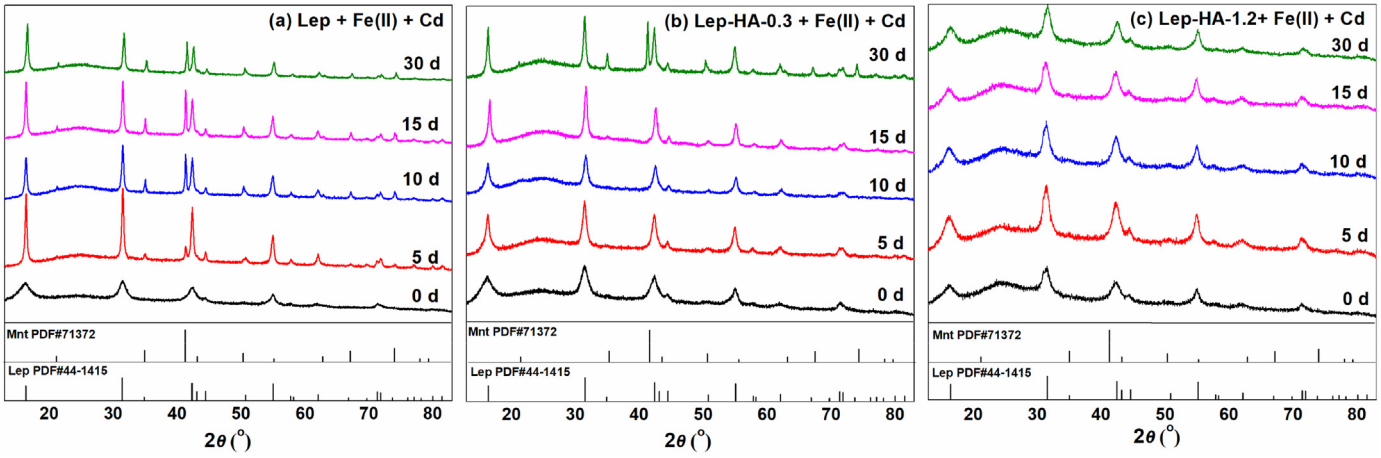

Fig. 2. XRD patterns of solid samples with Fe(II) and Cd(II) addition during reaction. (a) Lep + Fe(II) + Cd(II); (b) Lep-HA-0.3 + Fe(II) + Cd(II); (c) Lep-HA-1.2 + Fe(II) + Cd(II).

spectra of the Lep and Lep-HA-0.3 solid samples from the treatment with Fe (II) and Cd(II) after reaction for 30 days contain a doublet representing Lep and two broad and relatively symmetric sextets representing magnetite (including tetrahedral (A) site and octahedral (B) site) (Fig. 3d–e). These two treatments had similar compositions, containing 64.63 % and 72.41 % Lep and 35.37 % and 27.59 % magnetite, respectively (Table S1). This suggested that some of the Fe(II)$_{aq}$ was oxidized and entered into the structure of Lep, resulting in the formation of Lep and Magnetite. However, the presence of HA and Cd(II) had significant impacts on the IS values. Compared to the treatment without HA (Lep + Fe(II) + Cd(II)), the IS value of the A site magnetite increased and the IS value of the B site magnetite decreased in the presence of HA (Lep-HA-0.3 + Fe(II) + Cd(II)). The hyperfine magnetic field distributions of the magnetite under Cd(II)-free conditions increased in the low magnetic field compared to that of the Cd(II)-bearing treatments, providing evidence of the structural incorporation of Cd(II) during the Fe(II)-induced

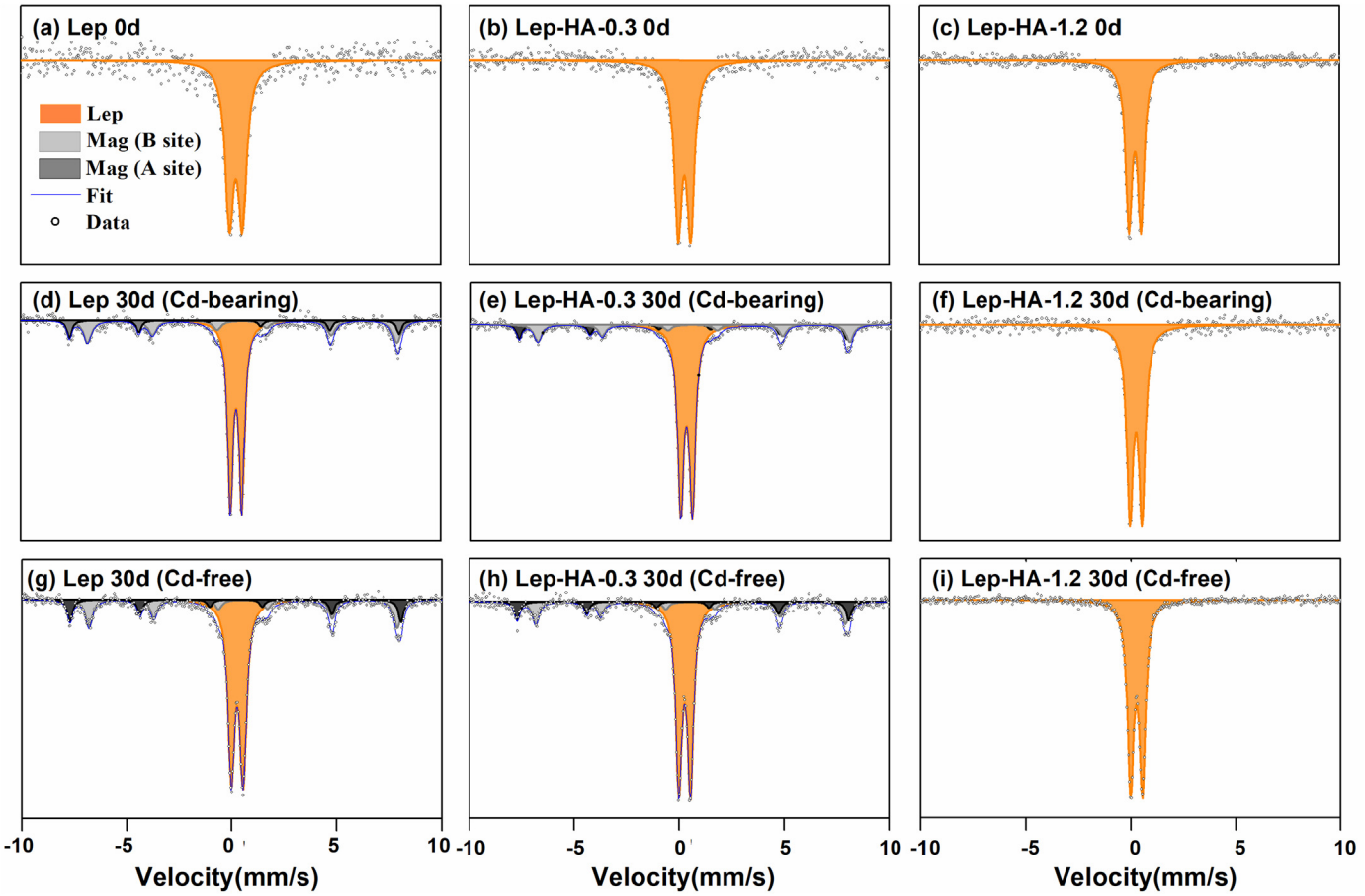

Fig. 3. Mössbauer spectra of solid samples before and after reaction with and without Cd(II) under the test condition of T = 295 k. (a–c) Solid samples at 0 day; (d–f) Solid samples reacted with Fe(II) and Cd(II); (g–i) Solid samples react with Fe(II) under the Cd-free condition. Black circle denotes the measured data. Red line denotes fitted data. Note: Lep = lepidocrocite; Mgt = magnetite.

transformation of Lep (Fig. 3, Table S1). Previous studies have shown that changes in the hyperfine magnetic field distribution of Fe minerals occur, and this could indicate the incorporation of additional metal cations into the structure (Huang et al., 2020). For the Lep-HA-1.2 treatments with Fe (II) and/or Cd(II), the spectra exhibited very similar characteristics for Lep after reaction for 30 days (Fig. 3f, i). Based on the above XRD results and Mössbauer analysis of these samples, it suggested that the presence of HA and Cd(II) affect the amounts and structure of the iron (oxyhydr)oxides during Fe(II)-induced Lep transformation.

The SEM images revealed that the morphology of the reacted solid samples differed depending on both the HA concentration and the spiked Fe(II) (Fig. S2). After reacting with the Fe(II) and Cd(II) for 30 days, the configuration of the Lep was destroyed and the morphology changed from short lath-like particles to spherical nano-sized magnetite particles with rough surface (Fig. 5a, d), indicating that Lep underwent reductive decomposition, which further resulted in the agglomeration of magnetite due to the magneto dipoles and Van der Wall forces (Rajput et al., 2016; Salazar-Camacho et al., 2013). The presence of HA resulted in the irregular shape and obvious agglomeration of iron (oxyhydr)oxides, and the morphology of the Lep-HA-0.3 and Lep-HA-1.2 treatments changed to rounded structures with a rough surface after reaction for 30 days (Fig. 5b–c, e–f). These differences in the morphology suggest that the transformation of the Lep was strongly altered by the presence of the HA and Cd(II). The energy-dispersive X-ray spectroscopy (EDS) analysis of the Lep-HA-1.2 samples after reaction for 30 days revealed the elemental distribution on the surfaces of the composites, and the main elements were Fe, O, and Cd (Fig. S3), suggesting that a close association between the Cd(II) and iron (oxyhydr)oxides. Similar results of Cd(II) enrichment on iron (oxyhydr)oxides in Fe-OM composites have been reported in a previous study (Qu et al., 2022).

Table 1
Binding energies (eV), assignments and quantification of O 1s XPS spectral bands of Lep and Lep-HA coprecipitates before and after Cd(II)/Fe(II) adsorption.

Treatments	Peak (eV)	Percentage (%)	Assignments
Lep	529.63	37.94	Fe-O-Fe
	530.88	51.15	Fe-O-H
	531.93	10.91	C-O-C
Lep + Cd(II)	529.55	42.5	Fe-O-Fe, Fe—O— Cd
	530.76	40.8	Fe-O-H
	531.45	16.7	C-O-C, C—O— Cd
Lep + Fe(II) + Cd(II)	529.51	36.59	Fe-O-Fe
	530.66	46.05	Fe-O-H
	531.53	17.36	C-O, C—O— Cd
HA	532.26	100	C=O
Lep-HA-0.3	529.76	29.89	Fe-O-Fe
	531.03	40.46	Fe-O-H, C-O
	532.36	29.65	C=O
Lep-HA-0.3 + Cd(II)	529.55	38.82	Fe-O-Fe
	530.81	49	Fe-O-H, Fe—O— Cd
	531.75	12.17	C-O
Lep-HA-0.3 + Fe(II) + Cd(II)	529.72	35.47	Fe-O-Fe
	530.97	52.98	Fe-O-H, C-O
	532.37	12.55	C=O
Lep-HA-1.2	529.68	29.7	Fe-O-Fe
	531	48.57	Fe-O-H, C-O
	532.38	21.73	C=O
Lep-HA-1.2 + Cd(II)	529.6	35.43	Fe-O-Fe
	530.92	54.6	Fe-O-H, Fe-O-Cd, C-O
	532.27	9.98	C=O
Lep-HA-1.2 + Fe(II) + Cd(II)	529.61	26.71	Fe-O-Fe
	530.92	46.19	Fe-O-H, C-O
	532.25	27.11	C=O, COO-Cd

3.3. Cd, O, and C speciation on reacted Fe-solid surface

XPS analyses was performed to identify the elements on the surface of the reacted Fe-solids phase. The full-scan spectra of the Lep and Lep-HA co-precipitates before and after reaction with Fe(II) and Cd(II) for 30 days are shown on Fig. S4. Almost all of the samples mainly contained C, O, and Fe, and a new Cd 3d peak appeared for the samples after the addition of Cd (II), demonstrating that the Cd (II) was successfully loaded onto the samples. According to Cd 3d spectra (Fig. 4), the two peaks at ~405.19 and ~411.96 eV, correspond to Cd $3d_{5/2}$ and Cd $3d_{3/2}$, respectively, indicating that the Cd(II) formed a Cd-OH complex with a hydroxyl group on the surface of the Lep or Lep-HA co-precipitates under the experimental conditions after 30 days (Guo et al., 2017; Ren et al., 2022; Zhang et al., 2016).

In the high-resolution spectrum of the O1s of the Lep (Table 1), the peaks at 529.63, 530.88, and 531.93 eV correspond to the oxygen bound in the crystal structure (Fe–O–Fe, ~529.63 eV), the oxygen on the surfaces (Fe-O-H, ~530.88 eV), and C—O (~531.93 eV), respectively (Xu et al., 2022). After reacted with Fe(II) and Cd(II) for 30 days, the Fe-O-Fe and Fe-O-H contents both slightly decreased. However, the component of C—O (~531.93 eV) increased from ~10.91 % to 17.36 % for the Lep, indicating that some of the C—O groups interacted with the Cd(II) and formed a Cd—O bond. After the addition of a low concentration of HA, the O 1 s XPS spectra of the Lep-HA-0.3 co-precipitate could be decomposed into three components, namely the oxygen bound in the crystal structure (Fe–O–Fe, ~529.76 eV), the oxygen on the surfaces (Fe-O-H or C—O, ~531.03 eV), and the oxygen in the HA (C═O, ~532.36 eV). Compared with the initial Lep sample, the non-lattice oxygen contents for Lep-HA-0.3 decreased, indicating that defects may have formed in the Lep after compositing with the low concentration HA, which was almost consistent with the XRD results. The peak area at ~531.03 eV increased from ~40.46 % to ~52.98 % for the Lep-HA-0.3 sample with Fe(II) and Cd(II), indicating that a proportion of the Fe-O-H groups interacted with the Cd(II). The surface ferric hydroxyl groups played a key role in the formation of Cd(II)

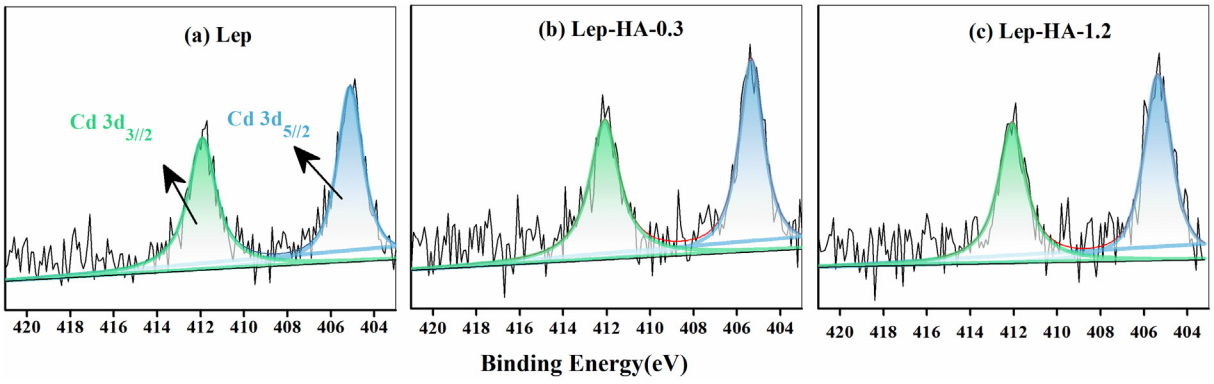

Fig. 4. XPS spectra of Cd 3d for Lep, Lep-HA-0.3 and Lep-HA-1.2 in the condition with Fe(II) and Cd(II) after reaction 30 days. The black lines denote the measured data. The red lines denote the smoothed data. Other lines denote XPS fitted spectra.

complexes on the Fe mineral surfaces, which is in agreement with the result of previous spectroscopic studies (Bao et al., 2021). However, for the Lep-HA-1.2 treatment, the surface ferric hydroxyl groups did not seem have a significant effect on the formation of the Cd(II) complexes. On the contrary, the contents of the C═O groups increased, also indicating that a proportion of the surface C═O groups interacted with the Cd(II). A previous study demonstrated that in a mixed Cd-amino acid solution, Cd(II) can form aqueous complexes with carboxyl groups (Xu et al., 2022). The Fe-O-Cd group formed in the Lep-HA co-precipitates after the addition of Cd(II) in Fe(II)-free treatment but it did not form in Fe(II)-bearing treatments. This may indicate that the Cd(II) tended to bind to the HA in the co-precipitates, but not to the hydroxyl group on the surface of the Fe minerals due to the competition with Fe(II) scince the affinity of Cd(II) for mineral surfaces is lower than that of Fe(II) at neutral pH (Bao et al., 2021; Zhao et al., 2022a, b; Zhou et al., 2020).

To further understand whether complexation occurred between the Cd(II) and the HA fraction, the C 1s spectra of the Lep-HA co-precipitate samples were analyzed. The C 1s XPS results revealed that the initial HA and Lep-HA co-precipitates exhibited three distinct peaks at 284.80, 286.48, and 288.50 eV (Fig. 5), corresponding to C-C/C-H in the aliphatic or amino acid side chains; C-O/C-N in the ether, alcohol, or amine; and C = O/O-C = O in the ketone or carboxyl groups, respectively (Guo et al., 2017). After reacted with Fe(II) and Cd(II) for 30 days, the percentages of the O-C = O group in the Lep-HA-0.3 and Lep-HA-1.2 decreased from 10.94 % to 7.04 %, and from 17.1 % to 9.04 %, respectively, suggesting that the O-C = O group participated in the adsorption process (Chen et al., 2020). Regarding to the Lep-HA co-precipitates, an increase in the C—O percentage was observed after the Fe(II) and Cd(II) treatments. This may have originated from the reaction between the C–OH and $Cd(OH)_2$, which formed an $(RCO)_2Cd$ species (Zhang et al., 2016).

3.4. Functional groups on reacted Fe-solid surface

FTIR analysis was conducted to investigate the changes in the functional groups of the Lep and Lep-HA co-precipitates before and after the reaction (Fig. 6). The assignments of each vibration (Table S3) were conducted based on previous reports (Gehring and Hofmeister, 1994; Gu et al., 2018; Rajput et al., 2016; Zhang et al., 2020). For all of the initial samples, three bands were observed at ~744, ~1022, and ~1155 cm^{-1}, which were attributed to the OH out-of-plane bending and OH in-plane bending (Gehring and Hofmeister, 1994), indicating the presence of Lep in the samples. During the reactions with Fe(II) and Cd(II), a shoulder band at 571 cm^{-1} appeared in the Lep spectra, which was attributed to the Fe—O stretching vibration of magnetite (Yuan et al., 2021). In addition, a new weak band at 521 cm^{-1}, attributed to Cd—O stretching (Saghatforoush et al., 2012), in the spectra of all of the samples, indicating the role of the O-containing groups in the Cd(II) adsorption (Fig. 6A). The disappearance of the OH-stretching of Lep (3381 cm^{-1}) after reacted with Fe(II) and Cd(II) reactions further revealed that the hydroxyl groups interacted with the Cd(II). A consistent red shift (from 3160 to 3055 cm^{-1}) was found in the treatment of Lep with Fe(II) and Cd(II) during the reaction, but this was not observed for the Fe(II)-free treatment. The band at ~3160 cm^{-1} was attributed to the hydrogen bonded OH-stretching of Lep. This red shift may be caused by the formation of more stable OH···O groups under the catalytic action of the Fe(II) (Jia et al., 2013). Some new bands (1975 and 1894 cm^{-1}) were observed for the Lep after the Cd(*II*)and Fe(II) reactions, and a new band (~1415 cm^{-1}), attributed to C—O stretching of the phenolic group (Huang et al., 2012), appeared for the Lep after the Cd(II) reaction without Fe(II), indicating that the organic functional groups interacted with the Cd(II).

For the Lep-HA-0.3 treatment, the FTIR results were almost the same as for the Lep samples. However, the hydroxyl groups disappeared until

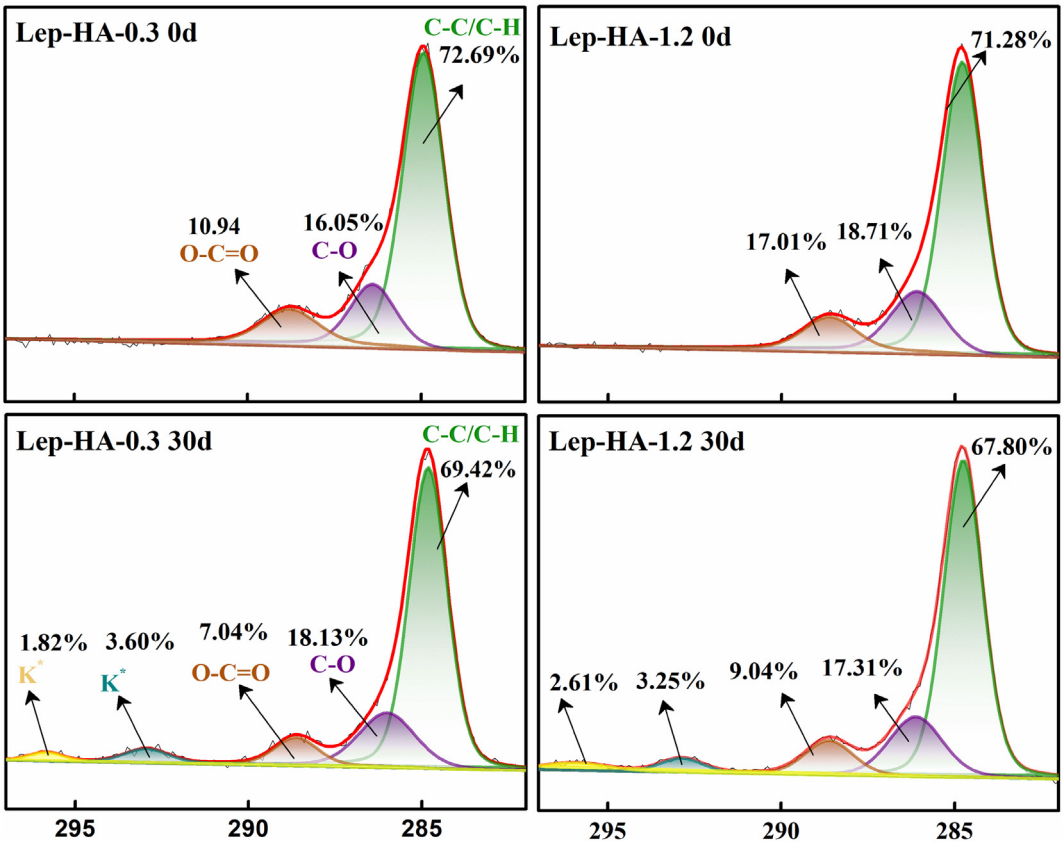

Fig. 5. (a) XPS spectra of C 1s for Lep-HA-0.3 and Lep-HA-1.2 before and after reacted with Fe(II) and Cd(II) 30 day. The black lines denote the measured data. The red lines denote the smoothed data. Other lines denote XPS-fitted fitted spectra. New peaks at 295.6 and 292.9 eV allocated to the K^+ ion in the KOH solutions.

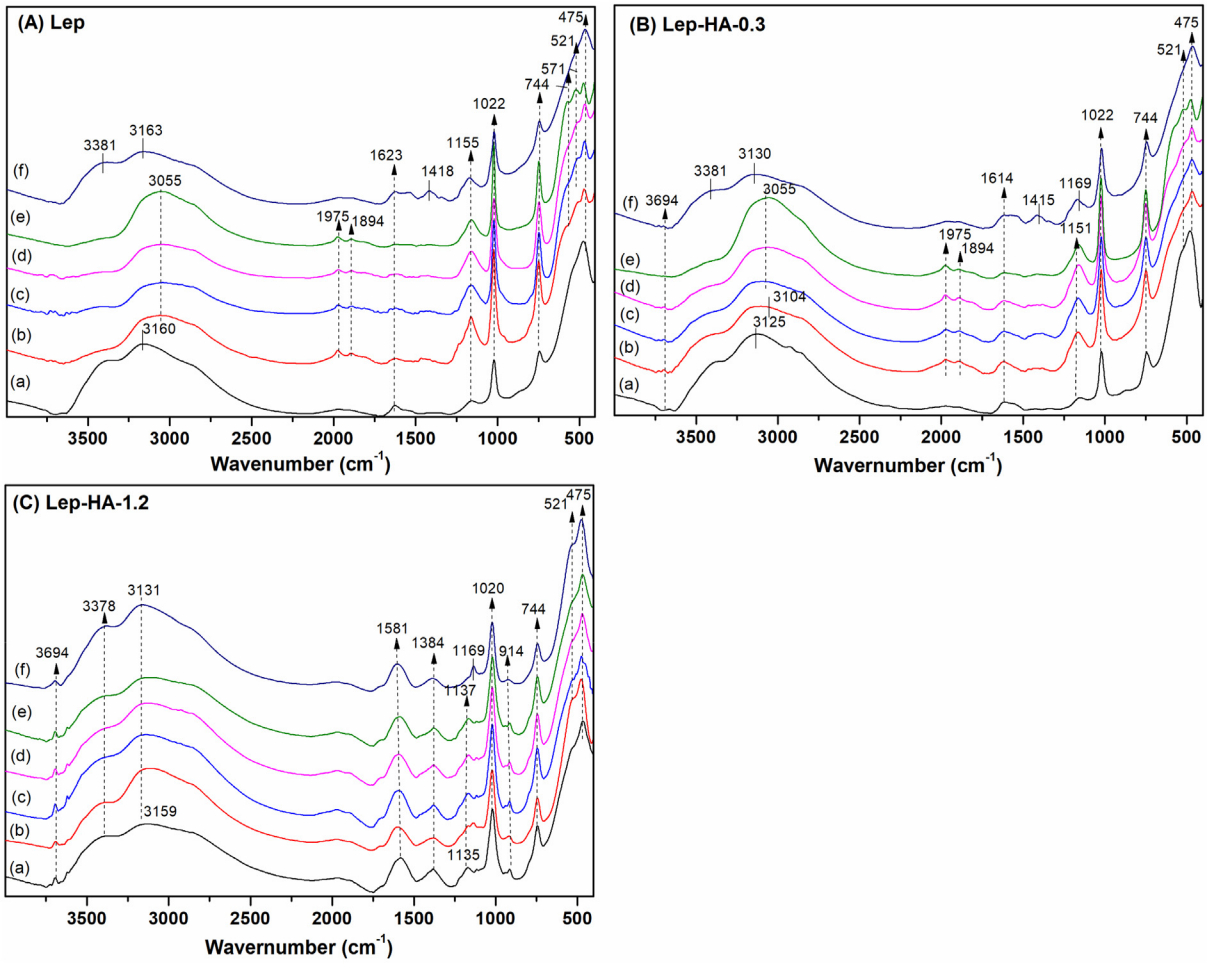

Fig. 6. FTIR spectra of Lep, Lep-HA-0.3, and Lep-HA-1.2 before and after Fe(II) and Cd treatment (labeled as sample-reaction time). (a) initial sample before reaction; (b–e) sample after Fe(II) and Cd reaction for 5, 10, 15 and 30 day; (f) sample after Cd reaction for 30 day in a Fe(II)-free condition.

30 days in the Lep-HA-0.3 treatment with Fe(II) and Cd(II) (Fig. 6B), indicating that the formation of magnetite promoted interactions between O-containing groups of the Fe minerals and the Cd(II). A shift (from 1151 to 1169 cm^{-1}) of the OH in-plane bending of the Lep was observed in the Lep-HA-0.3 treatment with Cd after reaction 30 days, which was ascribed to the surface complexation of Cd(II) to the -OH groups on the surface of the Lep-HA-0.3. However, this shift was not observed in the Lep and Lep-HA-0.3 treatments with Fe(II) and Cd(II) during the reaction, indicating that the HA made a major contribution to the interaction with the Cd(II) under Fe(II)-free conditions. The same shift (from 1135 to 1169 cm^{-1}) observed for the Lep-HA-1.2 treatment with Cd(II) after reaction for 30 days (Fig. 6C). Furthermore, the smaller red shift (from 3159 to 3131 cm^{-1}) of the Lep-HA-1.2 indicates that the co-precipitated HA with a higher C/Fe ratio inhibited the phase transformation of the Lep via the catalytic action of the Fe(II). The broad band at 3378 cm^{-1}, which was attributed to the O—H stretching bands of Lep-HA-1.2 after Fe(II) and Cd(II) treatment, remained almost invariant. Based on the above results, the occurrence of Cd—O stretching (521 cm^{-1}) suggested that the attachment of the Cd(II) to the Lep-HA-1.2 primarily occurred in the form of surface complexation of Cd(II) to the -OH groups on the surface of the HA.

3.5. Variation of dissolved and extracted Fe(II) concentration during Fe(II)-induced Lep-HA co-precipitates transformation

Previous studies have shown that the changes in the aqueous Fe(II) concentration induce a phase difference in iron (oxyhydr)oxides, and Fe (II) adsorption is the first step in the recrystallization of Lep to more crystalline Fe oxides (Hiemstra and van Riemsdijk, 2007). In this study, the concentration of the dissolved Fe(II) sharply decreased (Fig. 7a), while the concentration of the extractable Fe(II) increased after approximately 6 h for all of the samples (Fig. 7b), which was ascribed to the adsorption of Fe(II) by the Lep or Lep-HA co-precipitates. Fig. 7c shows that the aqueous Fe(II) available ability of the Lep and Lep-HA followed the order of Lep > Lep-HA-0.3 > Lep-HA-1.2. The zeta potential of Lep usually approaches zero at neutral pH, indicating that the surface is uncharged. Thus, suppressive Fe(II) adsorption of Lep-HA co-precipitates generally depends on changes in the surface charges and increases in the additional functional groups in Fe-solid samples (Du et al., 2018; ThomasArrigo et al., 2018). The suppression of Fe(II) adsorption prevents the recrystallization of Lep to more crystalline Fe oxides. Thus, magnetite was formed at 5 days for Lep alone, but it was not detected in the Lep-HA co-precipitates. Subsequently, the dissolved Fe(II) concentrations of the Lep-HA-1.2 steadily decreased toward the end of the experiment, while the dissolved Fe(II) concentrations of the Lep and Lep-HA-0.3 sharply decreased at 5 days and 15 days, respectively. This subsequent rapid decline may have been due to the formation of some newly formed Fe phases, e.g., magnetite crystal nuclei, which incorporated a large amount of Fe(II) into the lattice to participate in the subsequent mineralization process (Liu et al., 2022). This suggests that the HA both inhibited the exchange of iron atoms between Fe(II) and Lep and hindered the generation of the newly formed crystalline Fe phases. In addition, a slow increase of dissolved Fe(II) was observed for the Lep and Lep-HA-0.3 during 1–5 days (Fig. 7a) due to the changes in the specific surface area and particle size of the Fe-solid, which made the adsorbed Fe(II) unstable and stripped it from the surface as a results of the

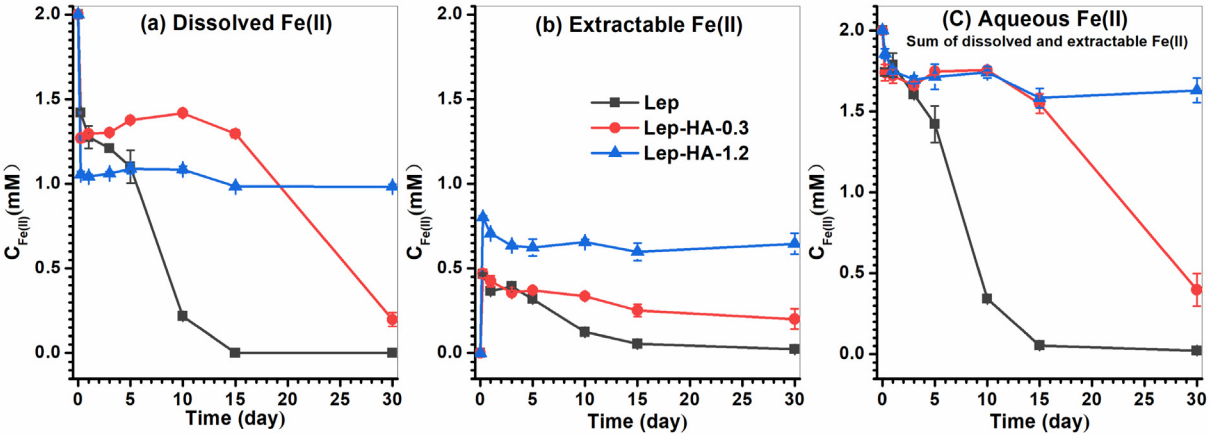

Fig. 7. Variation Trend of Fe(II) concentration ((a) dissolved Fe(II); (b) extractable Fe(II); and (c) aqueous Fe(II)) during the Fe(II)-induced Lep/Lep-HA transformation. Error bars represent one standard deviation of triplicate subsamples.

exchange of iron atoms between the Fe(II) and Lep (Zhou et al., 2020). The extractable Fe(II) concentration at the end of the reaction followed the order of Lep-HA-1.2 > Lep-HA-0.3 > Lep. However, in terms of early response, the highest extractable Fe(II) concentration occurred in the Lep-HA-1.2 treatment (Fig. 7b). These results indicate that the Fe(II) was complexed with the HA and thus suppressed the recrystallization of the Lep to more crystalline iron (oxyhydr)oxides. Overall, the HA had several effects on the Fe(II)-induced process: It adsorbed and complexed on Lep and formed dissolved complexes with the Fe(III) and Cd(II) (Fig. 7c), which thus inhibited the degree of atomic exchange between the labile Fe(II) and Fe(III) and prevented the recrystallization of the Lep to more crystalline iron (oxyhydr)oxides.

3.6. Mechanisms of the stabilization of Cd(II) during Fe(II)-induced Lep and Lep-HA co-precipitates transformation

The above results indicate that the mobility and distribution of Cd(II) on the solid surfaces were strongly controlled by HA during the transformation of Lep in the presence of Fe(II). HA bound to the Lep inhibited the transformation of the Lep to more crystalline phase magnetite. The mechanism of the Fe(II)-induced Lep transformation is believed to involve electron transfer between the added Fe(II) and structural Fe(III) and occurs via a dissolution–reprecipitation mechanism that is mediated by the Fe(II) (Liu et al., 2022). The presence of Fe(II) led to crystal dissolution and subsequent magnetite formation in the case of pure Lep. In OM-mineral composites, the chemical bonding and physically embedded or occluded species largely restrict the dissolution of the complexed Fe clusters (Kleber et al., 2015), which indicates the difficulty in the second phase transformation of the Lep-HA co-precipitates. In addition, the presence of HA increased the steric hindrance between the aqueous Fe(II) and labile Fe(III) due to the Fe(II) capturing ability of the carboxyl and hydroxyl functional groups (Sheng et al., 2020). This would result in occupation of the micropore passages or surface sites (Chen et al., 2014a), and impede the alignment and movement of the small clusters and the adhesion and formation of large aggregates (ThomasArrigo et al., 2019), which would further inhibit the formation of magnetite (Chen et al., 2015; Jones et al., 2009; Shen et al., 2022).

Interestingly, HA are very active soil components, particularly in cool, humid environments where an increase in COOH/Fe(II) ratios will influence the oxidative products of Fe(II) and lead to changes of iron (oxyhydr)oxides (Colombo et al., 2015). In this study, without HA, the Lep after 5 days of reaction produced large amounts of magnetite. In the presence of small amounts of HA (C/Fe = 0.3), the coprecipitation between Lep and HA probably modified the reaction pathways and electron transport, resulting in the formation of fewer magnetite. However, in the presence of large amounts of HA (C/Fe = 1.2), the Lep–HA coprecipitate inhibited the formation of magnetite. These showed that large amounts of HA have an obvious inhibitory effect on the formation of secondary mineralization.

Most certainly, the presence of Cd(II) under our experimental conditions did not alter the Lep transformation pathway induced by Fe(II). However, the presence of Fe(II) changed the the mobility of Cd(II) via inducing the transformation of Lep, and the presence of HA further affected the redistribution of the Cd(II) between the liquid and solids (Gu et al., 2018; Shen et al., 2022; Zhang et al., 2021). The mobility of heavy metals in iron (oxyhydr)oxides relies primarily on surface adsorption. The specific surface area of secondary iron (oxyhydr)oxides arisen from Fe(II)-induce transformation usually decreased with the conversion to more crystalline phases (Chen et al., 2015), leading to decrease of the surface adsorption sites of Cd(II). In addition, Cd(II) treatment experiment in this study was performed at neutral pH. For the Lep with Fe(II) and Cd(II) treatments, the sequestering of the Cd(II) probably occurred through the formation of hydroxyl-Cd (Figs. 4–5). The Cd(II) did not easily adsorb onto the iron (oxyhydr)oxides via electrostatic interaction at this pH.

For the Lep and Lep-HA-0.3 with Fe(II) and Cd(II) treatments, a portion of Cd(II) could be sequestered through structural substitution in newly formed Fe mineral except for above-mentioned surface binding. Based on Fig. 1, the Fe(II)-induced reaction promoted the immobilization of more Cd(II) ions, with ~63–69 % of the residual Cd(II) ions effectively stabilized by the mineral aggregates after the mineral transformation, indicating that more Cd(II) can be incorporated into secondary Fe minerals (Liu et al., 2016; Zhou et al., 2020). Mössbauer spectra also suggest the feasibility of the incorporation of Cd(II) into magnetite. Previous studies have even found that Cd, Cr, and As were gradually incorporated into the lattice structure of secondary Fe minerals under Fe(II)-induced ferrihydrite transformation (Hu et al., 2022; Shen et al., 2022; Yuan et al., 2021). The newly formed Fe mineral in the Lep and Lep-HA-0.3 treatments reflects a stable means of Cd(II) sequestration, which is possibly associated with structural incorporation or adsorption onto the defects in the Lep (Hu et al., 2022; Lu et al., 2019). In contrast, there was negligible magnetite formation before the migration of the Cd(II) into Fe-solid occurred, suggesting that the stabilization of Cd(II) primarily occurred through Lep aggregation prior the formation of the magnetite. Qu et al. (2022) also reported that the stabilization of Cd(II) occurred prior to hematite formation and primarily via ferrihydrite aggregation.

The mobility of Cd(II) in the Lep-HA co-precipitates was susceptible to high concentrations of HA (Fig. 1). The HA may have competed with iron (oxyhydr)oxides for the binding of the Cd(II) due to the fact that the co-precipitates have higher Cd(II) adsorption capacities than their individual constituents, except for HA (Vermeer et al., 1999; Liu et al., 2008;

Qu et al., 2022). In this study, the high HA concentration of the Lep-HA co-precipitates could promote the surface adsorption and immobilization of the Cd(II) ions in the suspension due to the negative charges and available adsorption sites. Similar phenomena has been observed by Lu et al. (2019), who found that Pb(II) adsorption by goethite-fulvic acid (FA) increased as the FA loading increased. The possible binding style may include Cd(II) as a "bridge" between the Lep and HA and or the Cd(II) directly bonded to the HA and the Fe-organic complexes on the Lep-HA co-precipitates (Orsetti et al., 2006). In the treatments with Fe(II), the high HA concentration increased the amounts of surface functional groups, whereas adsorption capacity of the Cd(II) ions were decreased. This was owing to the decrease of the specific surface area as a function of increasing C/Fe ratios (Chen et al., 2015). However, Fe(II) could have interact with the Lep-HA co-precipitates, which affected the reductive mineral dissolution and formation of a new mineral (Hu et al., 2022). It had further influenced the repartitioning of the Fe(II) and Cd(II) in the Lep-HA co-precipitates, and the phase transformation of the Fe minerals in this study. Based on the above results, the Cd(II) was fixed in the Lep-HA co-precipitates before transformation due to the effect of the HA, which resulted in the higher concentration of residual Cd(II) in the Lep-HA-0.3 treatment than in the Lep-HA-1.2 treatment. Thus, the amounts of extractable Cd(II) was higher than that of co-precipitate with small amounts of HA (C/Fe = 0.3) owing to surface complexes and incorporation (Hu et al., 2022). The lowest amounts of residual Cd(II) in Lep-HA-1.2 may be attributed to the inhibition of mineral phase transition, for that newly formed iron (Fe) (oxyhydr)oxides may immobilize Cd(II) through surface binding, structural substitution, and physical encapsulation (Hu et al., 2022). This phenomenon has also been reported for variation metal(loid)s, that is, a high valence-state metal(loid) would simultaneously be transformed into a low valence-state by the reductive functional groups of OMs (Du et al., 2018). However, there is currently a lack of knowledge regarding the HA sequestration stability of OM-Lep coprecipitates following Fe(II)-induced crystallization. Future studies to employ an OM component to determine organic carbon stability are highly recommended at both nano and molecular scales, for that whereas the presence of heavy metals promoted the generation of nano pore spaces or defects and consequently enhanced OM sequestration (Hu et al., 2022).

4. Conclusions

In this study, the stabilization of Cd(II) during the Fe(II)-induced transformation of Lep-HA co-precipitates under anaerobic conditions was studied. The results revealed that magnetite was formed during the Fe(II)-induced transformation of Lep and low C/Fe ratio Lep-HA co-precipitates, and the extent of the transformation decreased as the C/Fe ratios increased. HA bound to the Lep inhibited the transformation of Lep and further controlled the the mobility of Cd(II). The proportion of the extractable Cd(II) increased, while that of the the residual Cd(II) decreased as the HA concentration increased. The extractable and residual Cd(II) concentration in the Lep-HA co-precipitates was attributed to the presence of HA and the formation of magnetite induced by Fe(II), providing the surface sites of Cd(II) through surface binding, structural substitution, and physical encapsulation. A portion of Cd(II) have been immobilized by new-formed magnetite. These findings provide insights into the Cd(II) mobility in Fe minerals-OM in anaerobic environments via coupling of other redox and chemical processes.

CRediT authorship contribution statement

Hongling Bu: Investigation, Data curation, Formal analysis, Conceptualization, Writing – original draft, Writing – review & editing. **Qinkai Lei:** Investigation, Data curation, Formal analysis, Writing – review & editing. **Hui Tong:** Writing – review & editing. **Chengshuai Liu:** Funding acquisition, Methodology, Writing – review & editing. **Shujie Hu:** Writing – review & editing. **Wenpo Xu:** Writing – review & editing. **Yujie Wang:** Writing – review & editing. **Manjia Chen:** Supervision, Funding acquisition, Methodology, Writing – review & editing. **Jiangtao Qiao:** Writing – review & editing.

Data availability

No data was used for the research described in the article.

Declaration of competing interest

The authors declare that they have no known competing financial interests or personal relationships that could have appeared to influence the work reported in this paper.

Acknowledgement

We thank LetPub (www.letpub.com) for its linguistic assistance during the preparation of this manuscript. The research was supported by the Guangdong Basic and Applied Basic Research Foundation (Nos. 2021A1515011883 and 2019A1515011482), the National Key Research and Development Program of China (2020YFC1808500), the National Natural Science Foundation of China (Nos. 41977291, and 41907038), the GDAS' Project of Science and Technology Development (Nos. 2020GDASYL-20200102019, 2022GDASZH-2022010105, and 2020GDASYL-20200105002).

Appendix A. Supplementary data

Supplementary data to this article can be found online at https://doi.org/10.1016/j.scitotenv.2022.160624.

References

Bao, Y., Bolan, N.S., Lai, J., Wang, Y., Jin, X., Kirkham, M., Wu, X., Fang, Z., Zhang, Y., Wang, H., 2021. Interactions between organic matter and Fe (hydr) oxides and their influences on immobilization and remobilization of metal(loid)s: a review. Crit. Rev. Environ. Sci. Technol. 1–22.

Chen, C., Dynes, J.J., Wang, J., Sparks, D.L., 2014a. Properties of Fe-organic matter associations via coprecipitation versus adsorption. Environ. Sci. Technol. 48 (23), 13751–13759.

Chen, C., Kukkadapu, R., Sparks, D.L., 2015. Influence of coprecipitated organic matter on Fe2+ (aq)-catalyzed transformation of ferrihydrite: implications for carbon dynamics. Environ. Sci. Technol. 49 (18), 10927–10936.

Chen, M., Tao, L., Li, F., Lan, Q., 2014b. Reductions of Fe (III) and pentachlorophenol linked with geochemical properties of soils from Pearl River Delta. Geoderma 217, 201–211.

Chen, D., Wang, X., Wang, X., Feng, K., Su, J., Dong, J., 2020. The mechanism of cadmium sorption by sulphur-modified wheat straw biochar and its application cadmium-contaminated soil. Sci. Total Environ. 714, 136550.

Colombo, C., Palumbo, G., Sellitto, V.M., Cho, H.G., Amalfitano, C., Adamo, P., 2015. Stability of coprecipitated natural humic acid and ferrous iron under oxidative conditions. J. Geochem. Explor. 151, 50–56.

Cornell, R.M., Schwertmann, U., 2003. The Iron Oxides: Structure, Properties, Reactions, Occurrences, and Uses. 664. Wiley-VCH Weinheim.

Du, H., Peacock, C.L., Chen, W., Huang, Q., 2018. Binding of cd by ferrihydrite organo-mineral composites: implications for cd mobility and fate in natural and contaminated environments. Chemosphere 207, 404–412.

Ewing, F.J., 1935. The crystal structure of lepidocrocite. J. Chem. Phys. 3 (7), 420–424.

Frierdich, A.J., Catalano, J.G., 2012. Fe (II)-mediated reduction and repartitioning of structurally incorporated Cu, Co, and Mn in iron oxides. Environ. Sci. Technol. 46 (20), 11070–11077.

Gehring, A., Hofmeister, A., 1994. The transformation of lepidocrocite during heating: a magnetic and spectroscopic study. Clay Clay Miner. 42 (4), 409–415.

Gu, N.X., Oyala, P.H., Peters, J.C., 2018. An S= 1/2 iron complex featuring N2, thiolate, and hydride ligands: reductive elimination of H2 and relevant thermochemical Fe–H parameters. J. Am. Chem. Soc. 140 (20), 6374–6382.

Guo, Z., Zhang, J., Kang, Y., Liu, H., 2017. Rapid and efficient removal of Pb (II) from aqueous solutions using biomass-derived activated carbon with humic acid in-situ modification. Ecotoxicol. Environ. Saf. 145, 442–448.

Hiemstra, T., van Riemsdijk, W.H., 2007. Adsorption and surface oxidation of Fe (II) on metal (hydr) oxides. Geochim. Cosmochim. Acta 71 (24), 5913–5933.

Hu, S., Zhen, L., Liu, S., Liu, C., Shi, Z., Li, F., Liu, T., 2022. Synchronous sequestration of cadmium and fulvic acid by secondary minerals from Fe (II)-catalyzed ferrihydrite transformation. Geochim. Cosmochim. Acta 334, 83–98.

Huang, S.W., Chiang, P.N., Liu, J.C., Hung, J.T., Kuan, W.H., Tzou, Y.M., Wang, S.L., Huang, J.H., Chen, C.C., Wang, M.K., 2012. Chromate reduction on humic acid derived from a peat soil–exploration of the activated sites on HAs for chromate removal. Chemosphere 87 (6), 587–594.

Huang, H., Wang, J., Yao, R., Bostick, B.C., Prommer, H., Liu, X., Sun, J., 2020. Effects of divalent heavy metal cations on the synthesis and characteristics of magnetite. Chem. Geol. 547, 119669.

Jia, Y., Luo, T., Yu, X.Y., Sun, B., Liu, J.H., Huang, X.J., 2013. Synthesis of monodispersed α-FeOOH nanorods with a high content of surface hydroxyl groups and enhanced ion-exchange properties towards As (v). RSC Adv. 3 (36), 15805–15811.

Jing, F., Liu, Y., Chen, J., 2021. Insights into effects of ageing processes on Cd-adsorbed biochar stability and subsequent sorption performance. Environ. Pollut. 291, 118243.
Jones, A.M., Collins, R.N., Rose, J., Waite, T.D., 2009. The effect of silica and natural organic matter on the Fe (II)-catalysed transformation and reactivity of Fe (III) minerals. Geochim. Cosmochim. Acta 73 (15), 4409–4422.
Kappler, A., Bryce, C., Mansor, M., Lueder, U., Byrne, J.M., Swanner, E.D., 2021. An evolving view on biogeochemical cycling of iron. Nat. Rev. Microbiol. 19 (6), 360–374.
Karimian, N., Burton, E.D., Johnston, S.G., 2019. Antimony speciation and mobility during Fe (II)-induced transformation of humic acid-antimony (V)-iron (III) coprecipitates. Environ. Pollut. 254, 113112.
Kleber, M., Eusterhues, K., Keiluweit, M., Mikutta, C., Mikutta, R., Nico, P.S., 2015. Mineral–organic associations: formation, properties, and relevance in soil environments. Adv. Agron. 130, 1–140.
Latta, D.E., Bachman, J.E., Scherer, M.M., 2012. Fe electron transfer and atom exchange in goethite: influence of Al-substitution and anion sorption. Environ.Sci.Technol. 46 (19), 10614–10623.
Liu, J.-F., Zhao, Z.-S., Jiang, G.-B., 2008. Coating Fe3O4 magnetic nanoparticles with humic acid for high efficient removal of heavy metals in water. Environ. Sci. Technol. 42 (18), 6949–6954.
Liu, C., Zhu, Z., Li, F., Liu, T., Liao, C., Lee, J.-J., Shih, K., Tao, L., Wu, Y., 2016. Fe (II)-induced phase transformation of ferrihydrite: the inhibition effects and stabilization of divalent metal cations. Chem. Geol. 444, 110–119.
Liu, J., Sheng, A., Li, X., Arai, Y., Ding, Y., Nie, M., Yan, M., Rosso, K.M., 2022. Understanding the importance of labile Fe (III) during Fe (II)-catalyzed transformation of metastable iron oxyhydroxides. Environ. Sci. Technol. 56 (6), 3801–3811.
Lu, Y., Hu, S., Wang, Z., Ding, Y., Lu, G., Lin, Z., Dang, Z., Shi, Z., 2019. Ferrihydrite transformation under the impact of humic acid and Pb: kinetics, nanoscale mechanisms, and implications for C and Pb dynamics. Environ. Sci.: Nano 6 (3), 747–762.
Muehe, E.M., Obst, M., Hitchcock, A., Tyliszczak, T., Behrens, S., Schröder, C., Byrne, J.M., Michel, F.M., Krämer, U., Kappler, A., 2013. Fate of Cd during microbial Fe (III) mineral reduction by a novel and Cd-tolerant geobacter species. Environ. Sci. Technol. 47 (24), 14099–14109.
Murad, E., Schwertmann, U., 1984. The influence of crystallinity on the Mössbauer spectrum of lepidocrocite. Mineral. Mag. 48 (349), 507–511.
Orsetti, S., de las Mercedes Quiroga, M., Andrade, E.M., 2006. Binding of Pb (II) in the system humic acid/goethite at acidic pH. Chemosphere 65 (11), 2313–2321.
Qu, C., Chen, J., Mortimer, M., Wu, Y., Cai, P., Huang, Q., 2022. Humic acids restrict the transformation and the stabilization of Cd by iron (hydr) oxides. J. Hazard. Mater. 430, 128365.
Rajput, S., Pittman Jr., C.U., Mohan, D., 2016. Magnetic magnetite (Fe3O4) nanoparticle synthesis and applications for lead (Pb2+) and chromium (Cr6+) removal from water. J. Colloid Interface Sci. 468, 334–346.
Ren, J., Zheng, L., Su, Y., Meng, P., Zhou, Q., Zeng, H., Zhang, T., Yu, H., 2022. Competitive adsorption of Cd (II), Pb (II) and Cu (II) ions from acid mine drainage with zero-valent iron/phosphoric titanium dioxide: XPS qualitative analyses and DFT quantitative calculations. Chem. Eng. J. 445, 136778.
Saghatforoush, L.A., Sanati, S., Mehdizadeh, R., Hasanzadeh, M., 2012. Solvothermal synthesis of Cd (OH)2 and CdO nanocrystals and application as a new electrochemical sensor for simultaneous determination of norfloxacin and lomefloxacin. Superlattice. Microst. 52 (4), 885–893.
Salazar-Camacho, C., Villalobos, M., de la Luz Rivas-Sánchez, M., Arenas-Alatorre, J., Alcaraz-Cienfuegos, J., Gutiérrez-Ruiz, M.E., 2013. Characterization and surface reactivity of natural and synthetic magnetites. Chem. Geol. 347, 233–245.
Scheinost, A.C., Abend, S., Pandya, K.I., Sparks, D.L., 2001. Kinetic controls on Cu and Pb sorption by ferrihydrite. Environ. Sci. Technol. 35 (6), 1090–1096.
Schulz, K., ThomasArrigo, L.K., Kaegi, R., Kretzschmar, R., 2022. Stabilization of ferrihydrite and lepidocrocite by silicate during Fe (II)-catalyzed mineral transformation: impact on particle morphology and silicate distribution. Environ. Sci. Technol. 56 (9), 5929–5938.
Shen, X., Zhu, H., Wang, P., Zheng, L., Hu, S., Liu, C., 2022. Mechanistic and modeling insights into the immobilization of Cd and organic carbon during abiotic transformation of ferrihydrite induced by Fe (II). J. Hazard. Mater. 129216.
Sheng, A., Li, X., Arai, Y., Ding, Y., Rosso, K.M., Liu, J., 2020. Citrate controls Fe (II)-catalyzed transformation of ferrihydrite by complexation of the labile Fe (III) intermediate. Environ. Sci. Technol. 54 (12), 7309–7319.
ThomasArrigo, L.K., Byrne, J.M., Kappler, A., Kretzschmar, R., 2018. Impact of organic matter on iron (II)-catalyzed mineral transformations in ferrihydrite–organic matter coprecipitates. Environ. Sci. Technol. 52 (21), 12316–12326.
ThomasArrigo, L.K., Kaegi, R., Kretzschmar, R., 2019. Ferrihydrite growth and transformation in the presence of ferrous iron and model organic ligands. Environ. Sci. Technol. 53 (23), 13636–13647.
Vermeer, A.W., McCulloch, J.K., Van Riemsdijk, W.H., Koopal, L.K., 1999. Metal ion adsorption to complexes of humic acid and metal oxides: deviations from the additivity rule. Environ. Sci. Technol. 33 (21), 3892–3897.
Wang, P., Liu, K., Wang, X., Meng, Z., Xin, Z., Cui, C., Quan, F., Zhang, K., Xia, Y., 2022. Interface engineering of calligraphic ink mediated conformal polymer fibers for advanced flexible supercapacitors. J. Mater. Chem. A 10 (29), 15776–15784.
Xu, W., Liu, C., Zhu, J.-M., Bu, H., Tong, H., Chen, M., Tan, D., Gao, T., Liu, Y., 2022. Adsorption of cadmium on clay-organic associations in different pH solutions: the effect of amphoteric organic matter. Ecotoxicol. Environ. Saf. 236, 113509.
Yen, F.S., Chen, W.C., Yang, J.M., Hong, C.T., 2002. Crystallite size variations of nanosized Fe2O3 powders during γ-to α-phase transformation. Nano Lett. 2 (3), 245–252.
Yuan, Z., Zhang, G., Ma, X., Yu, L., Wang, X., Wang, S., Jia, Y., 2021. A combined abiotic oxidation-precipitation process for rapid as removal from high-As (III)-Mn (II) acid mine drainage and low as-leaching solid products. J. Hazard. Mater. 401, 123360.
Zhang, C., Yu, Z., Zeng, G., Huang, B., Dong, H., Huang, J., Yang, Z., Wei, J., Hu, L., Zhang, Q., 2016. Phase transformation of crystalline iron oxides and their adsorption abilities for Pb and Cd. Chem. Eng. J. 284, 247–259.
Zhang, J., Wang, X., Zhan, S., Li, H., Qiu, Z., 2020. Synthesis of Mg/Al-LDH nanoflakes decorated magnetic mesoporous MCM-41 and its application in humic acid adsorption. Microchem. J. 162 (3), 105839.
Zhang, M., Zhao, Z., Hui, B., Sun, J., Sun, J., Tian, W., Zhang, Z., Zhang, K., Xia, Y., 2021. Carbonized polymer dots activated hierarchical tungsten oxide for efficient and stable triethylamine sensor. J. Hazard. Mater. 416, 126161.
Zhao, X., Yuan, Z., Wang, S., Pan, Y., Chen, N., Tunc, A., Cheung, K., Alparov, A., Chen, W., Deevsalar, R., 2022. Iron (II)-activated phase transformation of Cd-bearing ferrihydrite: implications for cadmium mobility and fate under anaerobic conditions. Sci. Total Environ. 157719.
Zhao, X., Yuan, Z., Wang, S., Zhang, G., Qu, S., Wang, Y., Liu, S., Pan, Y., Lin, J., Jia, Y., 2022. The fate of co-existent cadmium and arsenic during Fe (II)-induced transformation of As (V)/Cd (II)-bearing ferrihydrite. Chemosphere 301, 134665.
Zhou, Z., Muehe, E.M., Tomaszewski, E.J., Lezama-Pacheco, J., Kappler, A., Byrne, J.M., 2020. Effect of natural organic matter on the fate of cadmium during microbial ferrihydrite reduction. Environ. Sci. Technol. 54 (15), 9445–9453.
Zhou, J., Liu, Y., Bu, H., Liu, P., Sun, J., Wu, F., Hua, J., Liu, C., 2022. Effects of Fe (II)-induced transformation of scorodite on arsenic solubility. J. Hazard. Mater. 429, 128274.